A calcium ion in a cavity as a controlled single-photon source

A calcium ion in a cavity as a controlled single-photon source

M Keller[1], B Lange[1], K Hayasaka[2], W Lange[1] and H Walther[1]

[1] Max-Planck-Institut für Quantenoptik, Hans-Kopfermann-Str. 1,
85748 Garching, Germany
[2] National Institute of Information and Communications Technology,
588-2 Iwaoka, Nishi-ku, Kobe 651-2492, Japan
E-mail: wfl@mpq.mpg.de

Abstract. We present a single calcium ion, coupled to a high-finesse cavity, as an almost ideal system for the controlled generation of single photons. Photons from a pump beam are Raman-scattered by the ion into the cavity mode, which subsequently emits the photon into a well-defined output channel. In contrast with comparable atomic systems, the ion is localized at a fixed position in the cavity mode for indefinite times, enabling truly continuous operation of the device. We have performed numeric calculations to assess the performance of the system and present the first experimental indication of single-photon emission in our set-up.

Contents

Institute *of* **Physics** Φ DEUTSCHE PHYSIKALISCHE GESELLSCHAFT

1. Introduction

The completely controlled emission of a single photon with high efficiency, externally triggered with a high repetition rate, is a goal pursued by a number of groups in atomic and solid-state physics. These efforts are motivated by a wide range of potential applications. Single photons provide a basis for secure quantum communication according to the method introduced by Bennett and Brassard [1], since they cannot be intercepted without irrevocably disturbing their quantum state. Similarly, optical quantum computation requires single photons as carriers of quantum information [2, 3]. An important prerequisite of a quantum-logic network [4] is the bidirectional mapping of quantum states between stationary atomic qubits and flying photonic qubits. It can be accomplished by reversing the process of single-photon generation, which is possible if it is based on the coherent interaction of an atom and a single field-mode. Beyond these practical applications, the pronounced non-classical properties of single-photon states make them ideal objects for fundamental investigations of quantum theory [5]–[7].

The applications cited above require a single-photon source with high efficiency and duty cycle and a strong suppression of two-photon emission events. In addition, the dynamics should be deterministic. The emission of the photon then occurs on demand, in response to a user-supplied trigger. Most quantum information processing schemes involve interference between the photons. The single-photon pulses should therefore occupy a well-defined spatio-temporal mode, with a Fourier-transform-limited spectrum.

A large number of experimental attempts have been made to build an efficient and deterministic single-photon source. Solid-state systems were realized, including PIN heterojunctions [8, 9], single-quantum dots [10]–[14] single molecules [15, 16] or single colour centres in nanocrystals [17, 18]. While producing antibunched light, these systems suffer from a combination of low efficiency, poorly defined output mode and a large spectral width of the output pulse. To increase the collection efficiency of single photons from quantum dots, microcavities have been employed recently [19, 20]. Still, the emission of the photons is not deterministically controlled. Moreover, it is an irreversible process and therefore cannot be employed to interface photonic to atomic quantum states. Single-photon states have also been generated with Rydberg atoms in microwave cavities [21]. In these micromaser experiments, however, the radiation remains confined to the resonator.

By contrast a single atom, strongly coupled to an optical cavity, can be used to produce single-photon pulses with high efficiency. The cavity defines an ideal Gaussian output mode and the bandwidth of the emitted pulse ideally is Fourier-transform-limited. This scheme for generating single-photon pulses was first proposed by Law and Kimble [22]. Recently, in a cavity quantum electrodynamics (CQED) implementation using atoms, the emission of up to seven photons was demonstrated [23]. Longer sequences were precluded by the finite dwell-time of the atom in the cavity region. Whereas the photon generation in the experiment is deterministic, a remaining element of randomness is the lack of control over the arrival of atoms in the cavity mode volume, which can only be determined by post-selection. In addition, the phase of the emission is randomized by the motion of the atom relative to the cavity mode.

The shortcomings of CQED with non-stationary atoms are avoided by using a single ion as an emitter. In contrast to atoms, ions can be readily localized in the cavity on a scale far below their resonance wavelength, as we have shown recently [24]. With ions, efficient and truly continuous emission of single photons is possible, without suffering from the low extraction efficiency of solid-state systems or the problems associated with non-stationary atoms in an optical cavity. By

using a Raman trigger-pulse, the properties of the generated photons can be deterministically engineered and by reversing the process it is possible to absorb the photon in the system in the same way.

The level structure of ions as well as the relevant system parameters are different from their atomic counterparts. In this paper, we present a theoretical model of single-photon generation with a single ion, providing a realistic description of a calcium ion coupled to a single-cavity mode. After introducing the system under study in section 2, we derive a master equation describing all processes relevant for single-photon production in section 3. The following sections discuss the results obtained from the model regarding the efficiency of single-photon generation (section 4) and the spectral properties of the photons (section 5). Finally, we give an overview of the experimental set-up and present first observations of single-photon emission from an ion-trap cavity–QED system (section 6).

2. Single-ion cavity–QED with calcium

Single trapped ions already have a remarkable history as sources of single photons. Since a single scatterer cannot emit a second photon immediately after it has been projected to the ground state in a previous emission process, the second-order correlation function $g^{(2)}(\tau)$ vanishes for zero time-delay τ. The phenomenon is known as photon antibunching and has been observed with ideal accuracy in resonance fluorescence of single ions [6, 25]. The anti-correlation of photon detections persists for a time determined by the Rabi frequency of the excitation. However, this set-up is of limited use for the deterministic delivery of photons. The main obstacle is that an ion in free space emits radiation into the full solid angle, so that only a small fraction may be captured and directed to the output port.

To enhance the coupling of the ion to a specific output mode, an optical cavity is needed. The interaction of a single atomic particle and the electromagnetic field in an optical resonator is the subject of cavity quantum-electrodynamics [26]. The most important parameter in the system is the rate of coupling $g(\boldsymbol{r})$ between atom and field, given by the dipole matrix element μ of the two-level atomic transition at frequency ω and the mode-distribution $f(\boldsymbol{r})$ in the cavity:

$$g(\boldsymbol{r}) = \sqrt{\frac{\mu^2 \omega}{2\hbar\epsilon_0 V_{\text{cav}}}} f(\boldsymbol{r}). \tag{1}$$

Here, $V_{\text{cav}} = \int |f(\boldsymbol{r})|^2 \, \mathrm{d}\boldsymbol{r}$ is the mode volume of the cavity, which should be small to achieve strong coupling.

As we have demonstrated previously [24], a single ion can be localized at the position $\boldsymbol{r}$ of maximum coupling for an indefinite time, so that the spatial variation of $g(\boldsymbol{r})$ may be neglected. This is an important advantage over atomic systems, where the randomness of the atoms' trajectories leads to large fluctuations in the coupling.

The efficiency of the cavity to deliver the photon to one of its output ports deteriorates in the presence of damping processes. Damping in the system can occur either by spontaneous decay of the upper atomic level to modes outside the cavity or by cavity losses. In the latter case, one should distinguish losses due to the finite transmissivity of the cavity mirrors and losses due to scattering or absorption in the mirrors. The transmission losses are the quantity actually being exploited when using the system as a single-photon source, since they result in
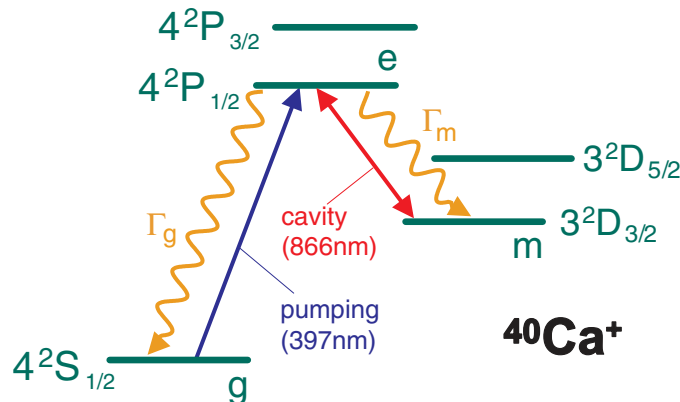
Figure 1. Level scheme of singly ionized ^{40}Ca$^+$. The transitions and decay rates between the levels (designated as *g*, *e* and *m*), which are relevant for the single-photon generation scheme described in this paper are indicated.

the emission of the photon to the output channel. Therefore, for high-efficiency single-photon generation, transmission losses should dominate cavity damping with a negligible contribution from scattering and absorption. This is a highly restrictive condition for an ion in a cavity. The reason is that the resonance transitions of ions have wavelengths in the ultraviolet region, where mirror losses are typically of the order of 10^{-3}. This value is comparable or even larger than the transmissivities needed for the realization of a CQED-based single-photon source. As a result, a photon in the cavity mode has only a small probability to escape to the output mode.

For an efficient single-ion photon source, transitions at longer wavelengths are required. They are available in some alkaline earth ions, in particular calcium and barium. They have metastable D-states, lying below the excited P-levels. In ^{40}Ca$^+$, the transition $4^2P_{1/2} \to 3^2D_{3/2}$ has a wavelength $\lambda = 866$ nm and thus falls in a region, where ultra-low loss mirror coatings are available. We have therefore chosen calcium as a suitable candidate for a single-photon source. A simplified level scheme of ^{40}Ca$^+$ is shown in figure 1, with the two decay rates Γ_g and Γ_m indicated.

Energy is delivered to the system by means of a pulsed pump laser on the $4^2S_{1/2} \to 4^2P_{1/2}$ resonance transition, which also serves as a trigger. A single photon is created by Raman scattering an ultraviolet photon from the pump beam, yielding an infrared photon in the cavity mode. The process leaves the ion in the state $D_{3/2}$, which is not coupled to the pump laser. Therefore, no additional photon is created in the pump cycle.

In the next section, the master equation of the driven system is solved to numerically investigate the process of single-photon generation.

3. Theoretical model: calcium ion coupled to a cavity mode

Using an atom coupled to an optical cavity to generate single-photon pulses was first proposed by Law and Kimble [22] and subsequently treated in a more general model by Kuhn *et al* [27]. In both cases, a scheme of three atomic levels *g*, *e* and *m* in a Λ-configuration, is considered, with a classical pulse $\Omega(t)$ driving the transition $|g\rangle \leftrightarrow |e\rangle$ and the cavity field coupled to the

transition $|m\rangle \leftrightarrow |e\rangle$ with strength g. We take this model as the starting point of our analysis. To accommodate the need for Doppler cooling of the ion, we include a detuning $\Delta = \omega_{\text{pump}} - \omega_{\text{eg}}$ of the pump-beam and a detuning $\delta = \omega_{\text{cav}} - \omega_{\text{em}}$ of the cavity from the respective atomic resonances. The Hamiltonian of the system in a frame of reference rotating at ω_{pump} and ω_{em} then is

$$H = \hbar\delta a^{\dagger}a + \hbar\Delta|g\rangle\langle g| + \hbar(\Omega(t)|e\rangle\langle g| + g|e\rangle\langle m|a + \text{h.c.}). \tag{2}$$

Here, the cavity mode is described by annihilation and creation operators a, $a^{\dagger}$. For a complete description of the system dynamics, atomic spontaneous emission into the ground state (at a rate Γ_g), the metastable state (at a rate Γ_m) and cavity losses (at a rate κ) must be included in the model. These processes are described by the master equation

$$\frac{\partial\rho}{\partial t} = -\frac{i}{\hbar}[H, \rho] + \kappa(2a\rho a^{\dagger} - a^{\dagger}a\rho - \rho a^{\dagger}a) + \frac{\Gamma_g}{2}(2|g\rangle\langle e|\rho|e\rangle\langle g| - |e\rangle\langle e|\rho - \rho|e\rangle\langle e|)\cdots$$

$$+\frac{\Gamma_m}{2}(2|m\rangle\langle e|\rho|e\rangle\langle m| - |e\rangle\langle e|\rho - \rho|e\rangle\langle e|). \tag{3}$$

In the two previous studies [22, 27], the coherent coupling rate g was assumed to be equal to or larger than the decay rates κ, Γ_g and Γ_m. This condition is not fulfilled in the ionic Λ-scheme we investigate here. The resonance transitions of *ions* are in the ultraviolet region and, hence, the upper P-level has a strong spontaneous decay rate Γ_g to the ground state. Decay on the pump transition is therefore the fastest rate in the system. In calcium, for example, $\Gamma_g = 2\pi \times 22\,\text{MHz}$, which is an order of magnitude larger than accessible values for the coupling g. Since spontaneous decay competes with the emission of radiation into the cavity, the large value of Γ_g seems to preclude the efficient production of single photons.

However, our calculations show that strong decay on the pump transition has only a negligible influence on the emission of single photons. The reason is that after a spontaneous transition back to the ground state, the ion will be re-excited by the pump pulse, until it finally makes a transition to the metastable state. The occurrence of multiple pump-decay cycles only slightly degrades the efficiency of single-photon generation.

The only relevant atomic damping process is spontaneous decay to the metastable state, since it irretrievably removes the ion from the pump cycle, a fact which prohibits the generation of more than one photon in the cavity. The decay rate on the infrared transition for calcium, $\Gamma_m = 2\pi \times 1.7\,\text{MHz}$, is small compared with the coherent coupling of the ion to the cavity, evolving at a rate g^2/κ. Efficient single-photon production with calcium ions is therefore possible.

The single-photon pulse profile, i.e. the time-dependent rate of emission from the cavity is obtained from the solution $\rho(t)$ of the master equation (3) by multiplying the cavity-mode occupation with the intensity transmission rate $2\kappa_t$:

$$P(t) = 2\kappa_t\,\text{Tr}\{a^{\dagger}a\rho(t)\}. \tag{4}$$

The efficiency of single-photon generation, i.e. the probability that a photon actually emerges from the cavity, is then simply obtained by integrating over the pulse profile:

$$\eta_{\text{pho}} = 2\kappa_t \int_0^{\infty} \text{Tr}\{a^{\dagger}a\rho(t)\}\,\text{d}t. \tag{5}$$
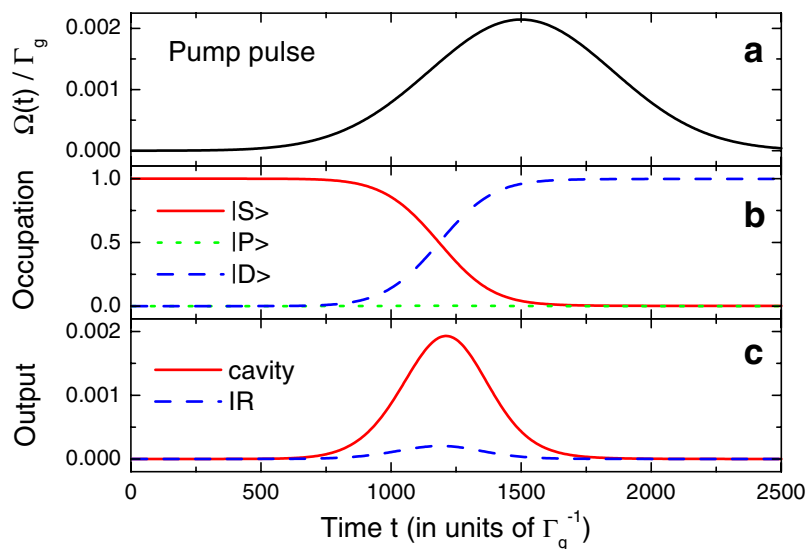
Figure 2. Single-photon generation in the three-level model: (a) driving pulse $\Omega(t)$, (b) evolution of atomic level occupation, (c) single-photon pulse $P(t)$ and the corresponding infrared fluorescence pulse. The parameters are $\kappa = 0.02\Gamma_g$, $g = 0.1\Gamma_g$, $\Delta = \delta = -0.15\Gamma_g$, $\Omega_0 = 0.11\Gamma_g$, $w = 500\Gamma_g^{-1}$ and $\kappa_t = 0.9\kappa$.

The rate κ_t only includes transmission through the mirror chosen as the output port. The total cavity decay rate κ also covers transmission through the other mirror and passive losses. These additional losses are proportional to the single-photon efficiency

$$\eta_{abs} = (\kappa/\kappa_t - 1)\eta_{pho}. \tag{6}$$

To obtain a high single-photon flux in one direction, the transmissivity of one mirror is made much larger than the other one. In this way, we define the output of the single-photon source. In our experiment, we have chosen 180 ppm for the output mirror and 10 ppm for the opposite mirror. In addition, absorption and scattering losses must be taken into account, which are minimized to 5 ppm by using highest-grade mirrors [28, 29]. Consequently, the photon in the cavity has a probability of 90% to be emitted through the output port ($\kappa_t = 0.9\kappa$), which is the upper limit of the single-photon generation efficiency of our device.

   The determination of the pulse shape $P(t)$ and the efficiency of single-photon emission requires a numerical solution of the master equation of the system. We start from an atom in the level $|g\rangle$ and an empty cavity. With a Gaussian pump pulse $\Omega(t) = \Omega_0 \exp(-(t - t_0)^2/2w^2)$ in the Hamiltonian (2) and typical system parameters, we obtain the solution presented in figure 2. According to equation (5), the efficiency is obtained by integrating over the output pulse shape $P(t)$, which is shown in the lower part of figure 2. In this example, the result is $\eta_{pho} = 82.1\%$.

   We have investigated the influence of strong spontaneous decay to the ground state by calculating output pulses for different values of the decay rate Γ_g. In each case, the driving field amplitude Ω_0 was chosen to maximize the efficiency. As can be seen from figure 3, the pulse shape is only minimally affected by Γ_g, as long as a suitable pump intensity is used. The inset to the figure shows that the required Ω_0 is proportional to the decay rate.

   The shape of the output pulse is largely determined by the shape of the driving pulse. For small pump amplitudes, the temporal profile of the single photon coincides with that of the pump
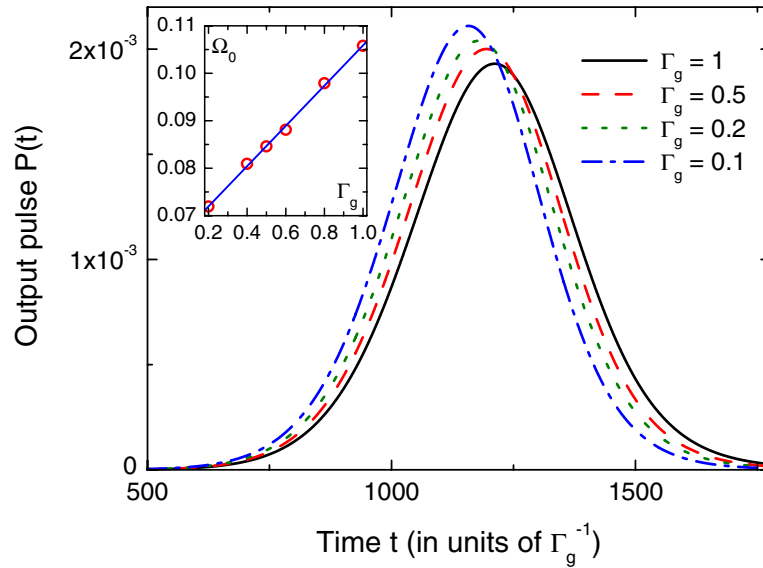
Institute *of* **Physics** Φ DEUTSCHE PHYSIKALISCHE GESELLSCHAFT

Figure 3. Pulse shape $P(t)$ for different decay rates Γ_g. The parameters are $\kappa = 0.02\Gamma_g$, $g = 0.1\Gamma_g$, $\Delta = \delta = -0.15\Gamma_g$ and $w = 500\Gamma_g^{-1}$. The values of Ω_0 were chosen to maximize the efficiency and are displayed in the inset.
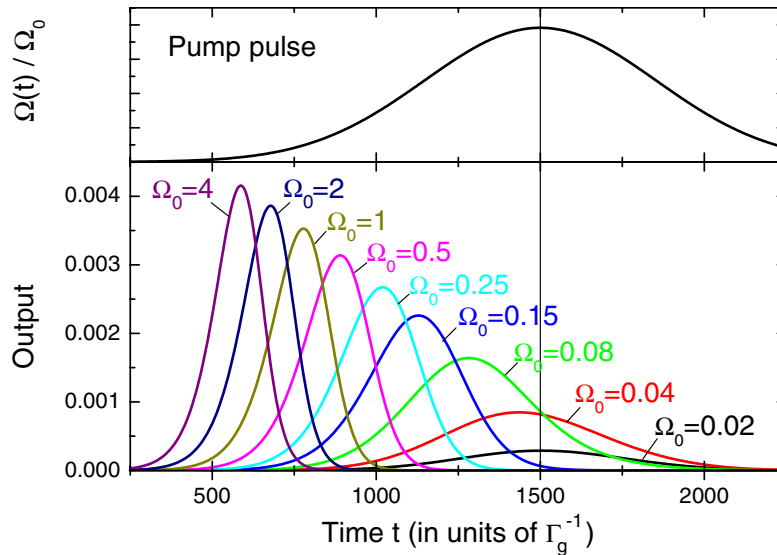
Figure 4. Pulse shape $P(t)$ for different amplitudes Ω_0 of the Gaussian pump pulse with width $w = 500\Gamma_g^{-1}$. The parameters are $\kappa = 0.02\Gamma_g$, $g = 0.1\Gamma_g$ and $\Delta = \delta = -0.15\Gamma_g$. As the pump intensity is increased, the output pulses become narrower and are emitted earlier with respect to the peak of the pump pulse.

pulse. When the amplitude Ω_0 of the pump field is large or the pulse width w is long, the photon is emitted from the cavity already during the leading edge of the pump pulse. In this case, the single-photon pulse is considerably shorter than the pump pulse. However, a lower limit for the width of the single-photon pulse is given by the inverse damping time of the cavity power, $1/2\kappa$. Photon pulses for different pump amplitudes are presented in figure 4.

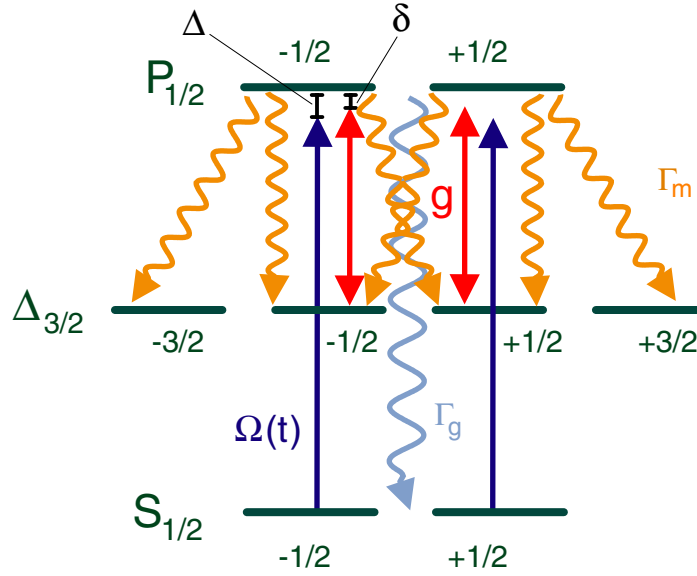**Figure 5.** Scheme of the eight-level model on which we base our numerical calculations. Pump and cavity field are assumed to be linearly polarized in the direction of the quantization axis. For clarity, the four possible sponataneous decay transitions to the ground state are represented by a single arrow. All couplings and decay rates have to be multiplied by Clebsch–Gordan coefficients.

From the solution of the master equation (3), we also obtain information on processes competing with single-photon emission. The probability for fluorescence emission on the infrared transition is calculated from the expectation value of the upper state occupation:

$$\eta_{\text{fluo}} = \Gamma_m \int_0^\infty \text{Tr}\{|e\rangle\langle e|\rho(t)\}\,\mathrm{d}t. \tag{7}$$

The infrared fluorescence pulse is also shown in figure 2. By evaluating equation (7) for the example, we find that 9% of the pump pulses result in infrared emission. Finally, there is a chance for the system to remain in the ground state at the end of the pulse:

$$\eta_0 = \lim_{t\to\infty} \text{Tr}\{|g\rangle\langle g|\rho(t)\}. \tag{8}$$

As can be seen from the evolution of the level occupations shown in figure 2(c), there is a negligible occupation of the state $|S\rangle$ at the end of the pulse ($\eta_0 \approx 0$). Since no other loss processes contribute, we have $\eta_{\text{pho}} + \eta_{\text{abs}} + \eta_{\text{fluo}} + \eta_0 = 1$.

In our set-up, the pump beam is also used to cool the thermal motion of the ion in the trap. Therefore, it must be red-detuned with respect to the atomic transition ($\Delta < 0$) to achieve Doppler cooling. In agreement with the results in [27], the cavity must be kept at Raman resonance with the driving field and therefore red-detuned as well.

A more realistic model has to take into account the Zeeman substates of the atomic levels, bringing their total number to eight. The complete level scheme is shown in figure 5. Since the excited state has only two sublevels, there is no cycling transition in the system. The coupling

between ion and cavity field is therefore reduced by a factor of $\sqrt{3}$ with respect to the three-level model. To avoid optical pumping through the driving field, linear polarization must be used for the S–P transition. The cavity supports two orthogonally polarized and degenerate TEM_{00} modes, either of which can receive the photon. Since the coupling rates for both modes are identical, we restrict our analysis to only one polarization mode, for simplicity, which we assume to be linear. In the actual experiment, the photons are unpolarized, but the emission rate is the same as the one calculated for a single polarization.

The atomic degrees of freedom in the multilevel system are described by operators A_σ, B_σ, which are composed of a sum over spin-$1/2$ operators for the Zeeman levels $|S_{1/2}, m_g\rangle$, $|P_{1/2}, m_e\rangle$ and $|D_{3/2}, m_m\rangle$ with weights corresponding to the Clebsch–Gordan coefficients for dipole coupling with polarization σ:

$$A_\sigma = \sum_{m_g, m_e} |S_{1/2}, m_g\rangle\langle S_{1/2}, m_g; 1\sigma|P_{1/2}, m_e\rangle\langle P_{1/2}, m_e|, \qquad \sigma = 0, \pm 1,$$

$$B_\sigma = \sum_{m_m, m_e} |D_{3/2}, m_m\rangle\langle D_{3/2}, m_m; 1\sigma|P_{1/2}, m_e\rangle\langle P_{1/2}, m_e|, \qquad \sigma = 0, \pm 1, \qquad (9)$$

$$m_g = \pm 1/2, \qquad m_e = \pm 1/2, \qquad m_m = \pm 1/2, \pm 3/2.$$

The Hamiltonian of the eight-level system is then given by

$$H = \hbar\delta a^\dagger a + \hbar\Delta \sum_{\sigma = 0, \pm} A_\sigma A_\sigma^\dagger + \hbar[\Omega(t) A_0^\dagger + ga B_0^\dagger + \text{h.c.}]. \qquad (10)$$

The master equation (3) is generalized to the eight-level case correspondingly. Again, the efficiency of single-photon generation is obtained from $\rho(t)$ according to equation (5). The infrared fluorescence probability is determined by summing over decay rates for the three possible polarizations:

$$\eta_{\text{fluo}} = \Gamma_m \int_0^\infty \text{Tr}\left\{ \sum_{\sigma = 0, \pm} B_\sigma^\dagger B_\sigma \rho(t) \right\} \, \mathrm{d}t. \qquad (11)$$

A basis for the Hilbert space of the atom–cavity system is provided by tensor products of the atomic states and the number states for the cavity mode. In this paper, we use the notation

$$|L_j, m_j, n\rangle = |L_j, m_j\rangle \otimes |n\rangle, \qquad L = \text{S, P, D} \qquad (12)$$

with j specifying the total angular momentum, $m_j = -j \ldots j$, the number of the magnetic sublevel and n the photon number in the cavity mode. Since in the scheme presented here, the cavity mode cannot contain more than one photon, we truncate the basis of photon states at $n = 2$.

An example of a calculation in the eight-level model is given in figure 6. As in figure 2, the evolution of level occupations, cavity output rate and infrared fluorescence intensity in response to a pump pulse with optimized amplitude are shown. Corresponding to equation (10), linearly polarized UV light and a linearly polarized cavity mode are used, so that the coherent driving only affects levels with magnetic quantum numbers $\pm 1/2$. In contrast, the levels $|D_{3/2}, \pm 3/2\rangle$ are populated entirely due to spontaneous transitions. The presence of additional decay channels reduces the single-photon efficiency with respect to the three-level case. In the following section, we analyse the issue of efficiency of single-photon generation in more detail.
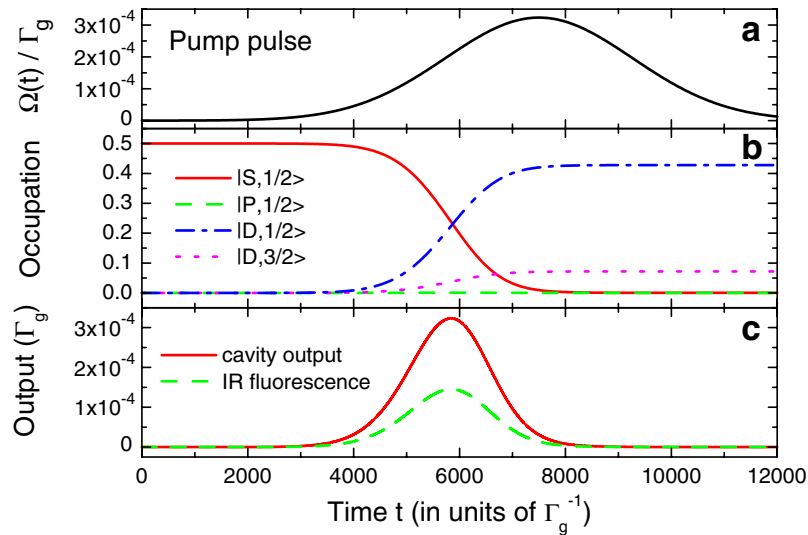
Figure 6. Single-photon generation in the eight-level model: (a) driving pulse $\Omega(t)$; (b) evolution of atomic level occupation: only magnetic Zeeman substates with $m_j > 0$ are shown, since the evolution is symmetric with respect to the sign of m_j; (c) single-photon pulse $P(t)$ and the corresponding infrared fluorescence pulse. The parameters are $\kappa_t = 0.1\Gamma_g$, $\kappa = 0.11\Gamma_g$, $g = 0.18\Gamma_g$, $\Omega_0 = 0.11\Gamma_g$, $\Delta = \delta = 0$ and $w = 2500\Gamma_g^{-1}$.

4. Efficiency of single-photon generation with a ^{40}Ca$^+$ ion

The fact that exactly one ion is interacting with the cavity and that the pump field is decoupled from the ion after a cavity photon is generated guarantees that not more than one photon is in the cavity mode at any time. Therefore, two photons can never be emitted from the cavity simultaneously. The essential figure-of-merit of an ion-trap single-photon source is then its efficiency, given by equation (5). It represents the probability of a single photon being ejected from the cavity as a result of a trigger pulse. In section 3, two processes have been identified, which lead to a reduced probability for photon emission: spontaneous decay of the ion to the metastable state, terminating the pump cycle without generating a photon in the cavity, and the ion remaining in the ground state at the end of the excitation pulse. We will now analyse in detail the dependence of these processes on the parameters of an ion-trap CQED system, with the goal of optimizing the efficiency for single-photon generation.

For a complete description of the experimental situation, we use the eight-level model and linearly polarized driving field and cavity mode. The parameters that most directly influence the ion–cavity interaction are the peak Rabi frequency Ω_0 of the driving field and the common detuning $\Delta = \delta$ of ion and cavity from the infrared resonance frequency (in the following we assume Raman resonance between ion and cavity). The efficiency of single-photon generation as a function of Ω_0 and Δ is shown in figure 7. The most striking feature is a sharp drop of the efficiency towards small values of Ω_0. In this case, the driving field is too weak to efficiently excite the ion and at the end of the trigger pulse it remains in the ground state with high probability. For large values of Ω_0 or Δ, increasingly strong infrared fluorescence is emitted at the expense of single-photon production. The optimum efficiency is reached at resonance ($\Delta = \delta = 0$) and
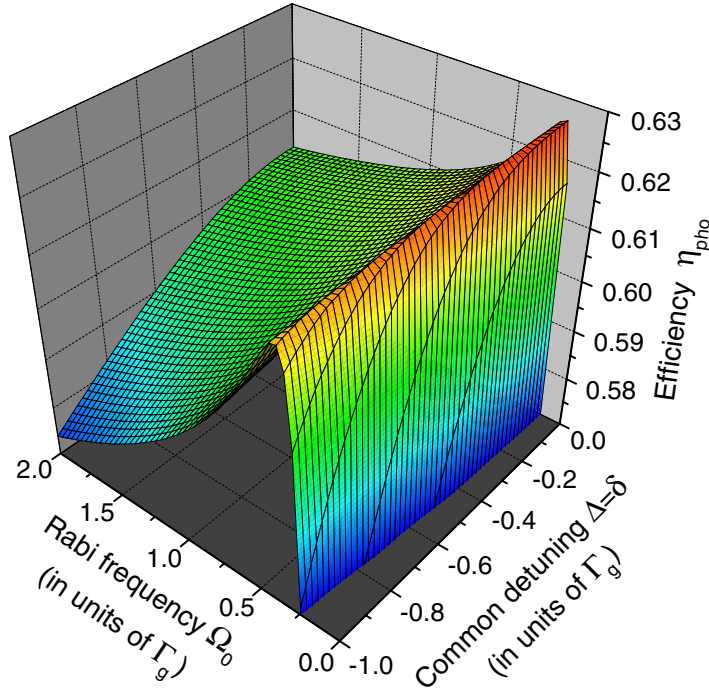
Institute *of* **Physics** Φ DEUTSCHE PHYSIKALISCHE GESELLSCHAFT

Figure 7. Single-photon efficiency as a function of the peak Rabi frequency Ω_0 of the pump field and the common detuning $\Delta = \delta$ of pump and cavity from the upper level in the case of Raman resonance. The coupling is chosen as $g = 0.18\Gamma_g$, whereas the cavity damping is $\kappa = 0.11\Gamma_g$. The pulse length is $w = 500\Gamma_g^{-1}$.

for a Rabi frequency roughly twice the effective coherent coupling, taking into account the Clebsch–Gordan coefficient ($\Omega_0 \approx 2g/\sqrt{3}$). In the calculations reported in the following, we have used zero detuning and the numerically determined optimum value of Ω_0. As mentioned above, in the experiment, the pump laser beam has the additional task to cool the ion's motion and should therefore be red-detuned ($\Delta \approx -\Gamma_g/2$). As can be seen from figure 7, the resulting drop in efficiency is only small.

In contrast with detuning and amplitude of the external driving field, the characteristic rates g, κ, Γ_g and Γ_m are fixed by the hardware of the system. Whereas the atomic decay rates are entirely determined by the ion species chosen, g and κ can be modified through the length L of the cavity:

$$g(L) = \sqrt{\frac{3c\lambda^2\Gamma_m}{8\pi V_{\text{cav}}}} \sim \frac{1}{L^{3/4}}, \qquad \kappa(L) = \frac{cT}{2L}, \tag{13}$$

where the volume V_{cav} was calculated for a TEM$_{00}$ mode of a Fabry–Pérot cavity and it was assumed that L is small compared with the radius of curvature of the mirrors. The parameter T describes the total losses of the cavity field. Figure 8 illustrates the length dependence of the three rates determining the dynamics of single-photon generation. For a cavity length between 0.1 and 3 mm, g is the largest rate in the system. For shorter values, cavity decay is dominant, whereas in a longer cavity, spontaneous decay is the main loss mechanism.
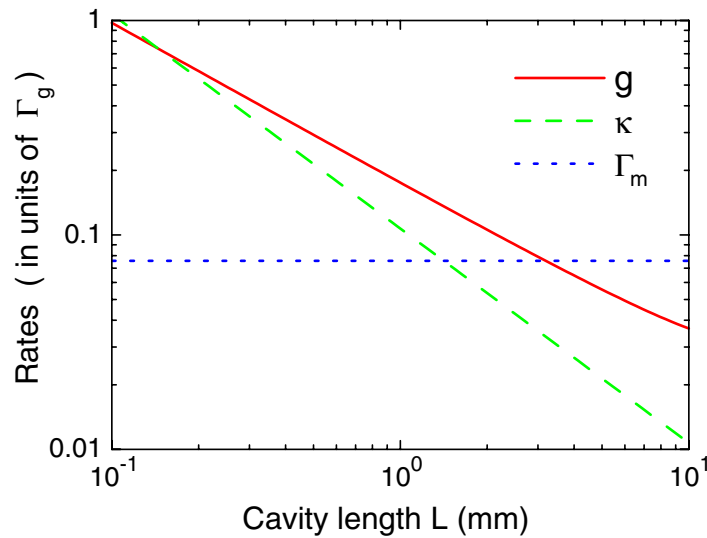
Figure 8. Characteristic rates of the cavity–QED system for a $^{40}\text{Ca}^+$-ion coupled to the cavity via the infrared transition. The overall mirror losses were taken to be 200 ppm and a radius of curvature of 1 cm was used.
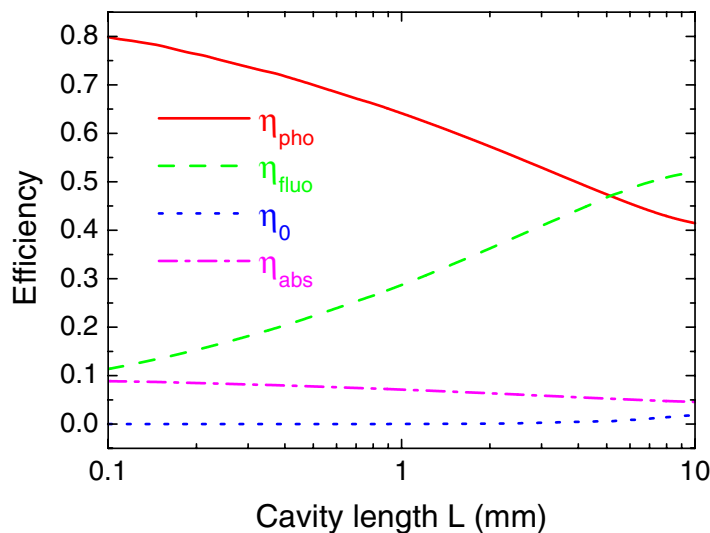

Figure 9. Single-photon efficiency (η_{pho}) and probability of fluorescence emission (η_{fluo}), ground-state occupation (η_0) and photon absorption (η_{abs}) as a function of cavity length. The parameters g and κ are obtained from figure 8. The pulse length was $w = 2500\Gamma_g^{-1}$. At each point, Ω_0 was chosen to optimize the efficiency.

The system parameters g and κ play a decisive role for the dynamics of single-photon generation. We have therefore investigated how the variation of these parameters with the cavity length L influences the efficiency of the process. For each value of L, we have maximized η_{pho} by choosing an optimum value of Ω_0. The resulting efficiencies for single-photon generation and the competing loss processes are shown in figure 9. Owing to the increased coupling g, the

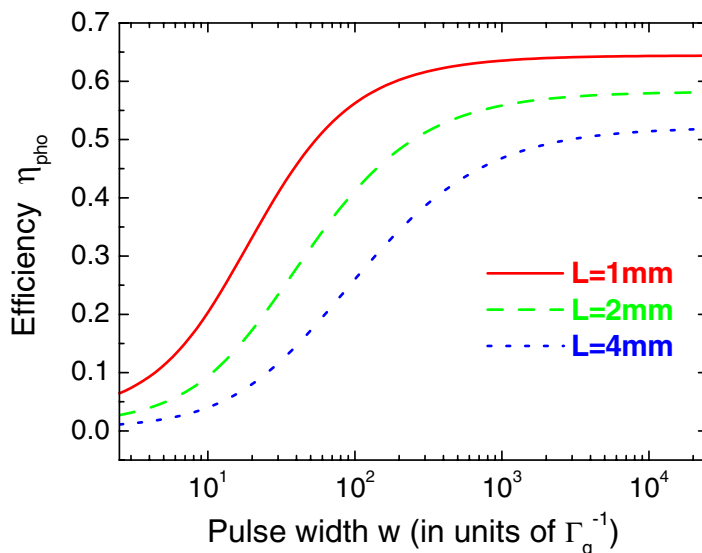Institute *of* **Physics** Φ DEUTSCHE PHYSIKALISCHE GESELLSCHAFT

Figure 10. Single-photon efficiency as a function of the width of the pump pulse. The three traces have been obtained for different sets of system parameters corresponding to three values of the cavity length L, determining the parameters g and κ (cf figure 8).

single-photon efficiency increases with decreasing L. To reach the limit of 90%, imposed by absorption and scattering losses in the mirror coatings, the cavity length must be reduced to below 0.1 mm. However, even for values between 1 and 10 mm, the efficiency of single-photon generation still reaches values between 40 and 60%. A good efficiency even for cavity lengths above 1 mm is of particular experimental relevance. The reason is that the radio-frequency field used for trapping the ion is strongly distorted, for a mirror distance in the sub-mm range, increasing the effort required for localizing the ion with sufficient precision.

In figure 4 it was shown that, within certain limits, the temporal structure of the output pulse is determined by the shape and amplitude of the pump pulse $\Omega(t)$. The time-scale set by the pump duration has also important implications for the efficiency of single-photon generation. This is apparent from figure 10, where the single-photon efficiency is plotted as a function of the pulse width w. Three sets of parameters are shown, corresponding to different values of the cavity length. Again, at each point, the amplitude Ω_0 of the pulse was optimized for efficiency. Evidently, the largest efficiencies are reached only if the pulse width exceeds a certain L-dependent threshold.

An explanation of this behaviour is provided by the concept of adiabatic population transfer [30]. This technique has already been applied successfully to the generation of single-photon pulses from atoms traversing a cavity [27, 31]. It is based on the adiabatic transformation of eigenstates of atom and field, achieved by changing the intensity of the driving field slowly compared with characteristic splittings (e.g. due to the ac-Stark effect) of the atomic energy levels. As a result, the system remains in the same eigenstate throughout the entire evolution. Particularly relevant is a class of states of the atom–cavity system called *dark states*, which include superpositions of ground states and metastable states, but no contribution from the decaying P-states.
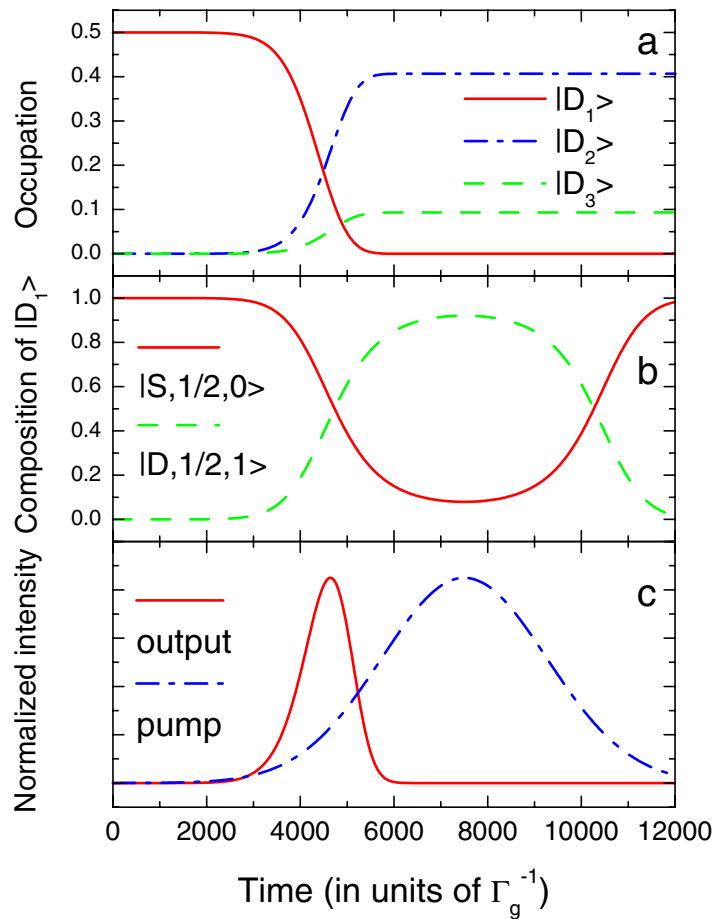
Figure 11. (a) Occupation of three relevant dressed states. (b) Composition of
the dressed state $|D_1\rangle$, showing a maximum contribution for a single-photon state
in the cavity at the peak of the pump pulse. (c) Normalized pump pulse and cavity
output. The latter is already terminated before the adiabatic process returns $|D_1\rangle$
to its initial composition.

The system evolution in the dressed state basis is illustrated in figure 11 for a calcium ion
and a linearly polarized pump pulse. In panel (a), the occupation probability of three relevant
dressed states is displayed as a function of time. At the beginning of the pulse, only the dressed
state $|D_1\rangle$ is occupied which coincides with $|S_{1/2}, 1/2, 0\rangle$. This is evident from panel (b) of
the figure, which shows the composition of dressed state $|D_1\rangle$ in terms of bare atomic states.
In the course of the driving pulse, $|D_1\rangle$ acquires a contribution from $|D_{3/2}, 1/2, 1\rangle$. While still
residing in the same eigenstate, the system has now a finite probability for a photon in the cavity.
Cavity losses induce a transition of the system to the dressed state $|D_2\rangle = |D_{3/2}, 1/2, 0\rangle$. In
addition, there is a small amount of residual spontaneous scattering to this state, as well as the
adjacent states $|D_{3/2}, -1/2, 0\rangle$ and $|D_{3/2}, 3/2, 0\rangle$ (not shown in the figure). In panel (c), pump-
and single-photon pulse are displayed for comparison. Evidently, the single-photon emission is
already terminated, when at the trailing edge of the pump pulse, the D-state contribution to $|D_1\rangle$
drops again. If the photon would still be in the cavity at this time, reabsorption would set in,
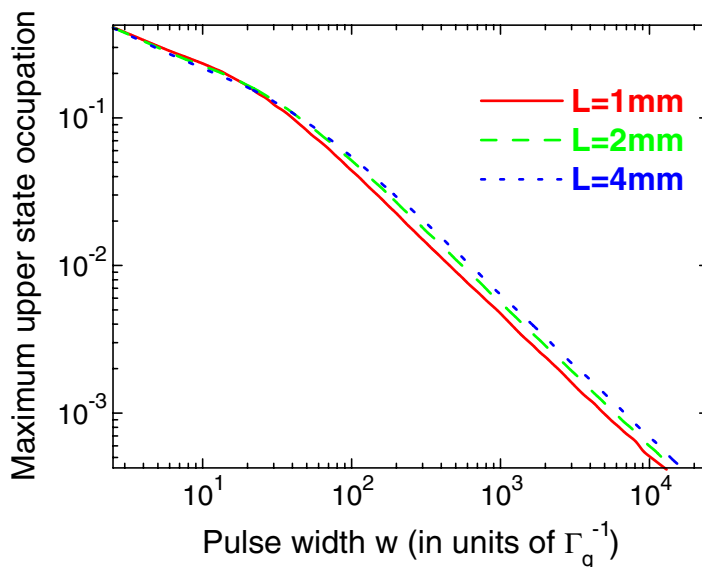lowering the efficiency of single-photon production.

Figure 12. Occupation of the upper state as a function of the width of the pump pulse. The drop can be attributed to the increasing adiabaticity as the pump pulse rises less steeply.

The essential feature of adiabatic population transfer, the reduced excitation of decaying levels, is clearly present in our solutions of the master equation of the system for different pulse widths. Figure 12 illustrates the reduction of population in the P-state, dropping to negligible values for longer pulses. It thus supports the interpretation of the increase of single-photon efficiencies with the pump-pulse width as the result of adiabatic dynamics, induced by the driving field.

For many applications, a high single-photon output rate may be more important than high efficiency in a single shot. The emission rate is limited by the duration of each photon pulse and the time it takes to recycle the ion to the initial state. For example, if a photon pulse with a FWHM of $10.000\Gamma_g^{-1}$ is generated, and assuming that it takes roughly twice as long to collect the entire pulse, the number of photons generated per second is limited to 7000, even at perfect efficiency. A better strategy to achieve a high single-photon flux is to reduce the pulse length and simultaneously increase the trigger rate. Even though the efficiency per pump pulse is slightly reduced (cf figure 10), this loss is overcompensated by the fact that triggering occurs at much higher frequency. Therefore, an overall increase in output rate results. In figure 13 we have calculated the output rates under the conditions that were used in figure 10. We have assumed that the output pulse is extracted in twice the FWHM of the pulse and that it takes $10\Gamma_g^{-1}$ to recycle the ion. For our parameters, the pulse length yielding the highest single-photon rates lies between 10 and $100\Gamma_g^{-1}$, depending on the length of the cavity.

A comparison with figure 10 shows that in the range, where the output rate is maximized, the single-photon generation efficiency is reduced to half its asymptotic value at large times. Our theoretical analysis shows that a single ion in a cavity can either be used as a highly efficient emitter of single photons, deterministically triggered one by one, or as a source producing a high flux of single photons.
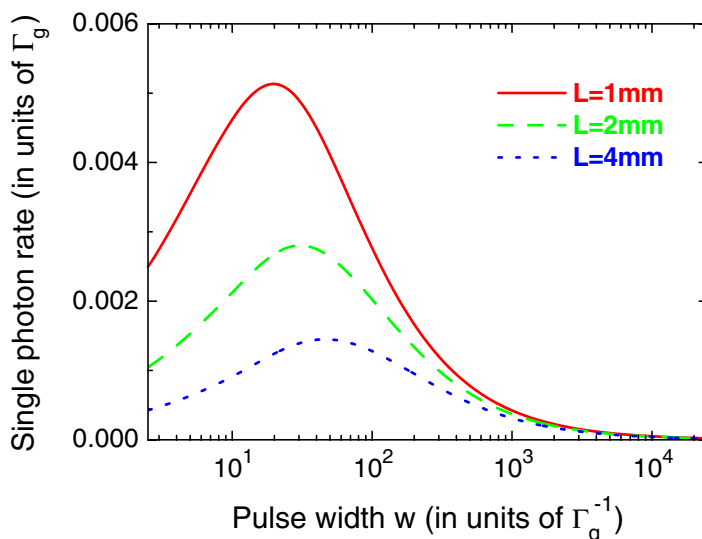
Institute *of* **Physics** ◉ DEUTSCHE PHYSIKALISCHE GESELLSCHAFT

Figure 13. Rates for single-photon generation, based on the results of figure 10. A pulse duration of twice the FWHM was assumed and a time of $10\Gamma_g^{-1}$ was added to accommodate recycling.

5. Single-photon spectra

The photon production efficiency is not the only important parameter characterizing a single-photon source. Equally relevant is the linewidth and spectral composition of the emitted photon pulse. Perfect interference of two single-photon pulses, for example, requires them to be indistinguishable, which can only be achieved if their spectrum is Fourier-transform-limited. This is a precondition for linear optics quantum computation schemes [3]. One of the great benefits of using trapped particles in cavities for the generation of single photons is that the output pulses are not subject to inhomogeneous line broadening and, ideally, should be Fourier-transform-limited.

To calculate the spectral properties of the photons generated with a calcium ion in a cavity, we have used the realistic eight-level model of section 3 to determine the spectrum of a single-photon pulse. Again we make the assumption that the pump and cavity mode are linearly polarized. For a non-stationary signal, the spectrum is defined via the correlation function of the cavity field:

$$S(\omega) = \frac{1}{2\pi} \int_{-\infty}^{\infty} dt_1 \int_{-\infty}^{\infty} dt_2 \langle a^\dagger(t_2) a(t_1) \rangle \, e^{-i\omega(t_2 - t_1)}. \tag{14}$$

The correlation function may be evaluated with the help of the quantum regression theorem. After Fourier transform with respect to the time difference and an integration over the remaining time coordinate, the spectrum $S(\omega)$ is obtained.

Three typical spectra for different pulse lengths are shown in figure 14. The lower trace, obtained with a short pump pulse, has a linewidth corresponding to the spectral width 2κ of the cavity. With increasing pulse length, the spectra become narrower, as expected for a Fourier-transform-limited pulse. The shape of the spectrum is, to a very good approximation, Lorentzian, whereas the temporal profile is closer to a Gaussian. It is important to verify how close the pulses come to the transform limit.
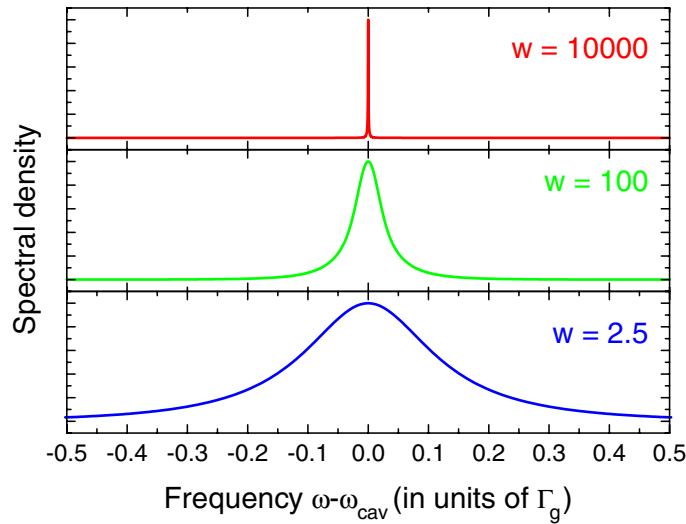
Institute *of* **Physics** Φ DEUTSCHE PHYSIKALISCHE GESELLSCHAFT

Figure 14. Spectra of single-photon pulses for three different widths of the pump pulse. The system parameters used are $g = 0.18\Gamma_g$, $\kappa = 0.11\Gamma_g$ and Ω_0 chosen to maximize the single-photon efficiency.
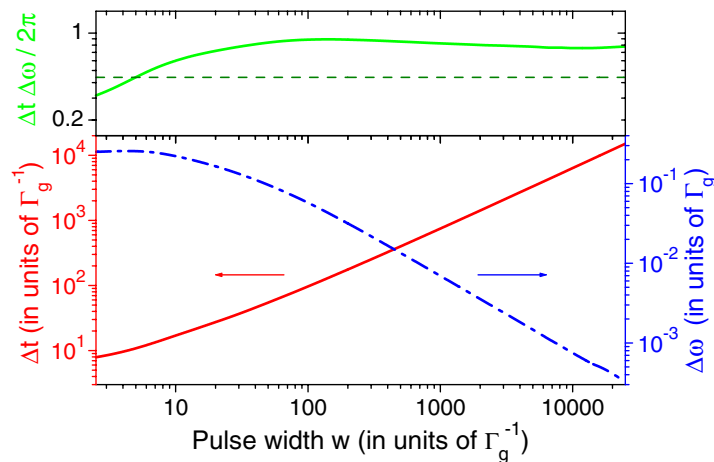

Figure 15. Calculated temporal FWHM and frequency bandwidth of single-photon pulses. The upper panel shows the time–bandwidth product. The dotted line indicates the time–bandwidth product of a transform-limited Gaussian pulse, which is $2\ln(2)/\pi$. The system parameters are the same as in figure 14.

To quantitatively compare the spectral and temporal profile of the pulses generated with our system, we have determined the FWHM-bandwidth $\Delta\omega$ of the spectrum $S(\omega)$ from equation (14) and the FWHM-width Δt of the pulse profile $P(t)$ obtained form equation (4). Both quantities are plotted as a function of pump-pulse width w in figure 15. The time–bandwidth product $\Delta t \cdot \Delta\omega$ of the pulses is shown in the upper panel of the figure. It stays nearly constant over four orders of magnitude of the pump-pulse width, demonstrating that the single-photon pulses are indeed transform limited with very good precision. The remaining variation of the time–bandwidth

product is due to the variation of the pulse shape as w is changed. The numerically determined results are within a factor of 2 of the value obtained for an ideal Gaussian shape, indicated by the dotted line in figure 15.

The subnatural linewidth of the single-photon spectrum, with values much smaller than the atomic decay rate Γ_m, in particular for long pulses, is based on the coherent nature of the Raman transition, leading to the excitation of a photon in the cavity mode. As shown in figure 12, in the case of long driving pulses, the maximum upper-state population in the Raman process is negligible. Therefore, the decay rate of the P-state has no bearing upon the spectral linewidth. Since the Raman transition connects two stable states, there is no lower bound for the linewidth other than the Fourier width connected with the finite pulse duration. It is instructive to compare the cavity output with the light emitted in the process of resonance fluorescence of a two-level atom in free space. If the excitation is weak, the fluorescent light is mainly due to coherent scattering and a narrow line is predicted in the spectrum [32, 33]. The effect has recently been observed with a single ion. In this case, the excitation was continuous, so that an infinitely narrow spectral line is expected. This narrow line was indeed observed experimentally by using heterodyne detection of the fluorescent light of a single ion [25]. Since only a single ion was used in this experiment, the photon statistics of the emitted light showed strong antibunching. In contrast, the single-photon source described in this paper is much more efficient, since all the photons are delivered to one well-defined output mode.

6. Experimental realization of cavity emission from a single ion

On the basis of the theoretical analysis presented in the previous sections, we have set up a trap for a single calcium ion coupled to a high-finesse cavity. The experiment is designed to operate in a parameter region suitable for the task of efficiently generating single photons.

A single calcium ion is confined in a linear radio-frequency trap. In the radial direction, a quadrupole potential is generated by four rf-electrodes, driven by a 400 V alternating voltage at a frequency of 12.7 MHz. In this way, harmonic confinement of the ion with an oscillation frequency $\omega_r/2\pi \approx 1.1$ MHz is reached. DC potentials applied to additional electrodes along the trap axis provide axial confinement and allow us to move the ion in and out of the cavity. Typical trapping lifetimes are of the order of hours, making continuous single-photon emission for long periods of time possible. The trap is described in more detail in [34].

The cavity mirrors are mounted with their axes perpendicular to the trap axis. By means of piezo-driven actuators, the distance of the mirrors to the ion and thus the cavity length L can be adjusted in a range of 0.8–10 mm. The radius of curvature of the mirrors is 10 mm. They taper to a diameter of 1 mm at the mirror surface, to facilitate laser access to the cavity centre and integration with the trap electrodes. A cross-section of the trap and the cavity region is shown in figure 16.

^{40}Ca$^+$ ions are created by photo-ionization of a neutral calcium beam [35, 36] in a loading region separated from the cavity centre by 25 mm. From there, a single ion is transferred to the cavity with the help of the dc electrodes. By tight confinement of the ion and laser Doppler cooling on the 397 nm transition (cf figure 1), we achieve a localization of the ion corresponding to a rms position spread of 42 nm [24], well in the Lamb–Dicke regime of the transition at 866 nm. Residual dc fields in the radial direction are carefully compensated with correctional voltages. Otherwise the ion would be pushed off the nodal line of the trapping field and undergo a driven
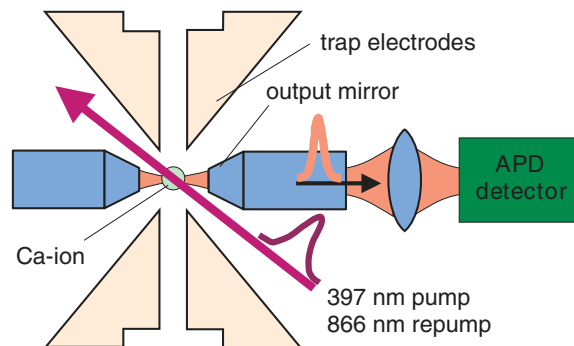
Figure 16. Experimental set-up for the generation of single-photon pulses with an ion–cavity system. The drawing shows a cross-section through the trap, perpendicular to the trap axis.

rf motion, resulting in a radial delocalization. After compensation of stray fields, a well-defined coupling g between ion and cavity field is guaranteed.

Two laser sources are required for the excitation of ^{40}Ca$^+$, as is apparent from figure 1. For the 4^2S$_{1/2} \rightarrow 4^2$P$_{1/2}$ transition, we use a frequency-doubled Ti : Sapphire laser at a wavelength of 397 nm. It is injected into the cavity region under an angle of 25° with respect to the trap axis. It has the principal task of providing the pump pulse for triggering single-photon emission. For this purpose, its intensity is controlled with an acousto-optic modulator. It is also used for Doppler cooling of the ion in the intervals between photon emissions. On the other transition of the calcium Λ-scheme, 4^2P$_{1/2} \rightarrow 3^2$D$_{3/2}$ at 866 nm, the photon is emitted. A laser at 866 nm is required for pumping the ion back to the ground state after each single-photon pulse and to avoid population trapping in the metastable D-level during Doppler cooling. In addition, this laser is needed to verify the correct tuning of the cavity before the experiment. We use an external grating stabilized diode laser, optically locked to a Cs-stabilized reference cavity to achieve a linewidth of less than 100 kHz.

We generate single photons by the following procedure: first, the ion is pumped to the ground state by illuminating it with the 866 nm laser for 0.5 μs. Subsequently, the driving pulse is injected, with a Gaussian temporal profile of 1 μs width and 300 μW peak intensity. After the single photon is emitted from the cavity (cf the calculated time profile of the photon pulse in figure 6), both lasers are switched on for 3 μs of Doppler cooling. This sequence is repeated at a rate of 100 kHz.

The single-photon pulses emanating from the output mirror in a Gaussian mode are focused on an avalanche photo-diode with a quantum efficiency specified as 26% at 866 nm. Single-photon emission critically depends on the cavity being tuned to Raman resonance with the pump pulse. This is demonstrated in the measurement reported in figure 17. It shows the rate of single-photon pulses as a function of cavity detuning, which has a pronounced peak at Raman resonance with the fixed frequency of the pump pulse. The figure is the first indication of single-photon emission in our system.

Figure 17 clearly shows that the cavity resonance has to stay well within the Raman resonance width of about 2 MHz for continuous single-photon generation. Although the cavity is located in a vacuum chamber, a large drift of the resonant frequency was observed. As a counter-measure, we are presently setting up an active lock of the cavity to a frequency-stabilized diode
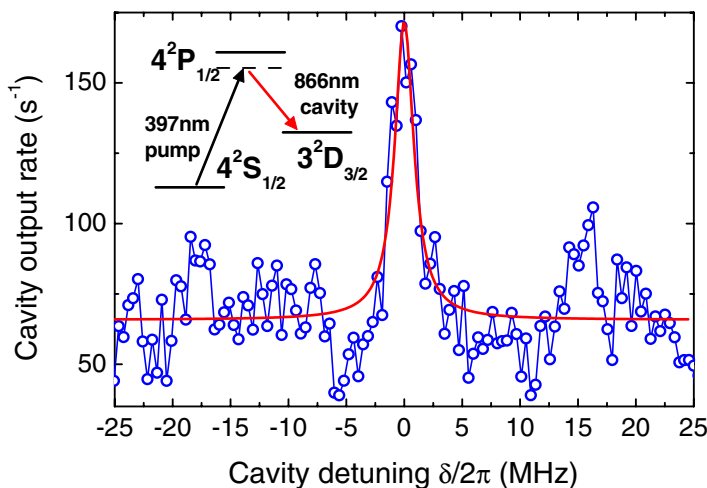
Figure 17. Measurement of the cavity emission as a function of the cavity detuning. The ion is pumped by pulses at 397 nm. Strong cavity output is observed at Raman resonance.

laser at 895 nm. Using a far-detuned wavelength is advantageous for distinguishing the generated single photons from the transmitted photons of the locking beam. By inserting a narrow bandwidth interference filter in front of the APD, the total detection efficiency at 895 nm is suppressed by a factor of 10^{-11} relative to that at 866 nm. This allows us to continuously lock the cavity to the 895 nm laser without adding background photons to the generated single photons at 866 nm. The 895 nm diode laser itself is stabilized by optical feedback [37], and is locked to the Cs D1-line [38]. We estimate the linewidth and long-term stability to be better than 200 kHz. The frequency of the 895 nm laser is shifted by means of an acousto-optic modulator and is matched to a resonant mode of the cavity. The cavity mode is chosen so that the 895 nm laser frequency and the centre frequency of the Raman line in figure 17 are simultaneously resonant with the cavity. This simple locking scheme keeps the cavity within the Raman resonance for hours. We will therefore be able to generate continuous trains of single-photon pulses for this period of time.

7. Conclusion

We have developed a model, realistically describing the interaction between a single ^{40}Ca$^+$ ion and a single mode of an optical cavity. Using the full Zeeman substructure of the atomic levels and including all relevant decay channels, we have integrated the master equation of the system and evaluated the time-dependent density matrix to calculate the cavity output as a function of time. We can therefore accurately predict the properties of the photon pulses emitted from the cavity.

By analysing the system dynamics in terms of dressed states of the system, we have shown that photon generation occurs as the result of an adiabatic process and therefore is more efficient for longer pump pulses. The adiabatic interaction has important implications for many aspects of the system behaviour. Due to the coherent character of the excitation, the spectral width of single-photon emission is only limited by the Fourier transform of the photon pulse, fulfilling

an essential requirement for a single-photon source in a photonic quantum computer. The strong spontaneous decay to the ground state, which is typical for ion systems, does not deteriorate the performance of single-photon generation, as long as the strength of the driving field is properly adjusted.

When the pump parameters are optimized, the maximum efficiency achievable in the system is determined by the coherent ion-field coupling g, which may be increased by reducing the cavity length. For a mirror separation of 0.1 mm, 80% efficiency is possible, which is close to the 90% upper limit set by passive cavity losses. For applications, in which a high single-photon output rate is required, shorter pump pulses and a higher duty cycle can be used.

Since we can keep an ion localized inside the cavity for many hours, our system has the capacity of truly continuous single-photon emission. Alternatively, the emission of the photon-pulse could be triggered on demand, taking advantage of the guaranteed presence of the ion in the armed state. The deterministic character of the ion–cavity interaction, together with high efficiency and a Fourier-limited spectrum makes our system an almost ideal source for single-photon emission.

Finally, we have presented an experimental set-up for a practical realization of an ion trap single-photon source, with first indications of single-photon emission.

References

[1] Bennett C H and Brassard G 1984 *Proc. IEEE Int. Conf. on Computers, Systems and Signal Processing, New York* p 175
[2] Turchette Q A, Hood C J, Lange W, Mabuchi H and Kimble H J 1995 *Phys. Rev. Lett.* **75** 4710
[3] Knill E, Laflamme R and Milburn G J 2001 *Nature* **409** 46
[4] Cirac J I, Zoller P, Kimble H J and Mabuchi H 1997 *Phys. Rev. Lett.* **78** 3221
[5] Kimble H J, Dagenais M and Mandel L 1977 *Phys. Rev. Lett.* **39** 691
[6] Diedrich F and Walther H 1987 *Phys. Rev. Lett.* **58** 203
[7] Nogues G, Rauschenbeutel A, Osnaghi S, Bertet P, Brune M, Raimond J M, Haroche S, Lutterbach L G and Davidovich L 2000 *Phys. Rev.* A **6205** 054101
[8] Kim J, Benson O, Kan H and Yamamoto Y 1999 *Nature* **397** 500
[9] Imamoglu A and Yamamoto Y 1994 *Phys. Rev. Lett.* **72** 210
[10] Michler P, Kiraz A, Becher C, Schoenfeld W V, Petroff P M, Zhang L D, Hu E and Imamoglu A 2000 *Science* **290** 2282
[11] Santori C, Pelton M, Solomon G, Dale Y and Yamamoto E 2001 *Phys. Rev. Lett.* **86** 1502
[12] Santori C, Fattal D, Vuckovic J, Solomon G S and Yamamoto Y 2002 *Nature* **419** 594
[13] Yuan Z L, Kardynal B E, Stevenson R M, Shields A J, Lobo C J, Cooper K, Beattie N S, Ritchie D A and Pepper M 2002 *Science* **295** 102
[14] Zwiller V, Aichele T, Seifert W, Persson J and Benson O 2003 *Appl. Phys. Lett.* **82** 1509
[15] Basche T, Moerner W E, Orrit M and Talon H 1992 *Phys. Rev. Lett.* **69** 1516
[16] Lounis B and Moerner W E 2000 *Nature* **407** 491
[17] Kurtsiefer C, Mayer S, Zarda P and Weinfurter H 2000 *Phys. Rev. Lett.* **85** 290
[18] Beveratos A, Kuhn S, Brouri R, Gacoin T, Poizat J P and Grangier P 2002 *Eur. Phys. J.* D **18** 191
[19] Moreau E, Robert I, Gerard J M, Abram I, Manin L and Thierry-Mieg V 2001 *Appl. Phys. Lett.* **79** 2865
[20] Pelton M, Santori C, Solomon G S, Benson O and Yamamoto Y 2002 *Eur. Phys. J.* D **18** 179
[21] Brattke S, Varcoe B T H and Walther H 2001 *Phys. Rev. Lett.* **86** 3534
[22] Law C K and Kimble H J 1997 *J. Mod. Opt.* **44** 2067
[23] Kuhn A, Hennrich M and Rempe G 2002 *Phys. Rev. Lett.* **89** 067901
[24] Guthöhrlein G R, Keller M, Hayasaka K, Lange W and Walther H 2001 *Nature* **414** 49

[25] Höffges J T, Baldauf H W, Lange W and Walther H 1997 *J. Mod. Opt.* **44** 1999
[26] Berman P R (ed) 1994 *Cavity Quantum Electrodynamics. Advances in Atomic, Molecular and Optical Physics*
        Suppl. 2 (San Diego, CA: Academic)
[27] Kuhn A, Hennrich M, Bondo T and Rempe G 1999 *Appl. Phys.* B **69** 373
[28] Rempe G, Thompson R J, Kimble H J and Lalezari R 1992 *Opt. Lett.* **17** 363
[29] Hood C J, Kimble H J and Ye J 2001 *Phys. Rev.* A **64** 033804
[30] Parkins A S, Marte P, Zoller P and Kimble H J 1993 *Phys. Rev. Lett.* **71** 3095
[31] Hennrich M, Legero T, Kuhn A and Rempe G 2000 *Phys. Rev. Lett.* **85** 4872
[32] Weisskopf V 1931 *Ann. Phys. (Leipzig)* **9** 23
[33] Mollow B R 1969 *Phys. Rev.* **188** 1569
[34] Keller M, Lange B, Hayasaka K, Lange W and Walther H 2003 *Appl. Phys.* B **76** 125
[35] Gulde S, Rotter D, Barton P, Schmidt-Kaler F, Blatt R and Hogervorst W 2001 *Appl. Phys.* B **73** 861
[36] Lucas D M, Ramos A, Home J P, McDonnell M J, Nakayama S, Stacey J-P, Webster S C, Stacey D N and
        Steane A M 2004 *Phys. Rev.* A **69** 012711
[37] Hayasaka K 2002 *Opt. Commun.* **206** 401
[38] Udem T, Reichert J, Holzwarth R and Hansch T W 1999 *Phys. Rev. Lett.* **82** 3568